



HAL
open science

Unstable and stable regimes of polariton condensation

F. Baboux, D. de Bernardis, V. Goblot, V. Gladilin, C. Gomez, E. Galopin, L. Le Gratiet, A. Lemaître, I. Sagnes, I. Carusotto, et al.

► **To cite this version:**

F. Baboux, D. de Bernardis, V. Goblot, V. Gladilin, C. Gomez, et al.. Unstable and stable regimes of polariton condensation. *Optica*, 2018, 5 (10), pp.1163. 10.1364/OPTICA.5.001163 . hal-02353534

HAL Id: hal-02353534

<https://hal.science/hal-02353534>

Submitted on 7 Oct 2022

HAL is a multi-disciplinary open access archive for the deposit and dissemination of scientific research documents, whether they are published or not. The documents may come from teaching and research institutions in France or abroad, or from public or private research centers.

L'archive ouverte pluridisciplinaire **HAL**, est destinée au dépôt et à la diffusion de documents scientifiques de niveau recherche, publiés ou non, émanant des établissements d'enseignement et de recherche français ou étrangers, des laboratoires publics ou privés.



Distributed under a Creative Commons Attribution 4.0 International License



Unstable and stable regimes of polariton condensation

F. BABOUX,^{1,2,*}  D. DE BERNARDIS,^{3,4,5} V. GOBLOT,¹ V. N. GLADILIN,³ C. GOMEZ,¹ E. GALOPIN,¹ L. LE GRATIET,¹ A. LEMAÎTRE,¹  I. SAGNES,¹  I. CARUSOTTO,⁴  M. WOUTERS,³ A. AMO,¹ AND J. BLOCH¹

¹Centre de Nanosciences et de Nanotechnologies, CNRS, Univ. Paris-Sud, Université Paris-Saclay, C2N–Marcoussis, F-91460 Marcoussis, France

²Laboratoire Matériaux et Phénomènes Quantiques, Université Paris Diderot, CNRS-UMR 7162, Paris 75013, France

³TQC, Universiteit Antwerpen, Universiteitsplein 1, B-2610 Antwerpen, Belgium

⁴INO-CNR BEC Center and Dipartimento di Fisica, Università di Trento, I-38123 Povo, Italy

⁵Vienna Center for Quantum Science and Technology, Atominstytut, TU Wien, 1040 Vienna, Austria

*Corresponding author: florent.baboux@univ-paris-diderot.fr

Received 27 December 2017; revised 22 March 2018; accepted 22 April 2018 (Doc. ID 318096); published 24 September 2018

Modulational instabilities play a key role in a wide range of nonlinear optical phenomena, leading, e.g., to the formation of spatial and temporal solitons, rogue waves, and chaotic dynamics. Here, we experimentally demonstrate the existence of a modulational instability in condensates of cavity polaritons, quasi-particles arising from the strong coupling of cavity photons with quantum well excitons. For this purpose, we investigate the spatiotemporal coherence properties of polariton condensates in GaAs-based microcavities under continuous-wave pumping. The chaotic behavior of the instability results in a strongly reduced spatial and temporal coherence and a significantly inhomogeneous density. Additionally, we show how the instability can be tamed by introducing a periodic potential so that condensation occurs in negative mass states, leading to largely improved coherence and homogeneity. These results pave the way to the exploration of long-range order in dissipative quantum fluids of light within a controlled platform.

Published by The Optical Society under the terms of the [Creative Commons Attribution 4.0 License](https://creativecommons.org/licenses/by/4.0/). Further distribution of this work must maintain attribution to the author(s) and the published article's title, journal citation, and DOI.

OCIS codes: (030.1640) Coherence; (160.6000) Semiconductor materials; (190.5970) Semiconductor nonlinear optics including MQW; (020.1475) Bose-Einstein condensates.

<https://doi.org/10.1364/OPTICA.5.001163>

1. INTRODUCTION

Modulational instabilities are a widespread feature of nonlinear wave systems, whereby small perturbations get amplified and grow exponentially with time. They manifest in numerous branches of physics ranging from hydrodynamics [1] to nonlinear optics [2], plasma physics [3], and cold atom gases [4]. In optical systems such as fibers [2,5], waveguide arrays [6], lasers [7–9], and amplifiers [10], modulational instabilities have been shown to deeply affect the temporal or spatial properties of light fields, leading, e.g., to the breakup of uniform beams into trains of solitons [6,11], the generation of filaments [12], or the emergence of extreme intensity fluctuations known as optical rogue waves [9,13]. Chaotic dynamics related to instabilities have been especially studied in lasers [9,14] with envisioned applications in random number generation and optical sensing [8].

Cold atom condensates, where the sign and strength of nonlinearities can be dynamically tuned using Feshbach resonances [15,16], have also been a fruitful playground for the experimental investigation of instabilities. A homogeneous cold atom condensate becomes unstable in the presence of attractive interactions, which make the condensate collapse so as to minimize its

potential energy [17,18]. In the presence of a confining potential, however, zero-point kinetic energy competes with interactions, and a condensate can persist up to a given critical density [19] after which the condensate implodes [16,20] or breaks into a train of solitons [4,21]. Inspired by dispersion management techniques used in fiber optics to generate solitons or gap solitons [22–24], self-bound condensate droplets have also been observed for repulsively interacting atoms when the atomic effective mass is turned to negative by means of an optical lattice [25] or of a spin-orbit coupling [26]. For non-equilibrium systems, however—such as in the presence of drive and dissipation—the fate of the instability of bosonic condensates has been little explored experimentally so far.

Polaritons, arising from the strong coupling of quantum well excitons and cavity photons [27], are an appealing candidate to address this question. These quasi-particles indeed combine non-equilibrium properties with substantial interactions. Direct interactions between polaritons are of repulsive nature [28], which should preclude the aforementioned instability scenario. However, under the widely used non-resonant pumping scheme, interactions between polaritons and the reservoir cloud of

uncondensed excitons need also to be considered. This polariton–reservoir coupling can be shown to give effective *attractive* interactions between condensed polaritons [29,30]. When these effective interactions overcome the direct repulsive interactions between polaritons, the condensate is expected to enter a modulationally unstable regime [31] characterized by a turbulent steady state [29,30,32–34]. This behavior strongly contrasts the collapse scenario of attractively interacting cold atom gases and is another intriguing example of the rich non-equilibrium physics of driven-dissipative polariton condensates.

While predicted a decade ago [31] this instability of polariton condensates has been hindered in previous experimental reports, except for a recent study using organic cavities under pulsed excitation [35]. Here, we evidence the presence of instabilities in the most typical case of *inorganic* cavities and under *continuous-wave* (CW) pumping, and we highlight how their signatures are markedly distinct from the ones observed in Ref. [35]. We also demonstrate a method to suppress the polariton instability. For this purpose, we investigate the coherence properties of polariton condensates in 1D and 2D GaAs-based cavities in which the sign of the polariton effective mass can be changed. When condensation occurs in a positive mass state, we observe an unstable steady state regime characterized by a strongly reduced spatial and temporal coherence, and a sizable density inhomogeneity. When the cavities are spatially patterned into lattices so that condensation occurs in negative mass states, the modulational instability is suppressed, and all previous signatures of instability disappear: the condensates reach a stable steady state with high homogeneity and coherence. This method for suppressing instabilities opens avenues for studying the rich phenomenology of driven-dissipative condensates [36–43], such as Kardar–Parisi–Zhang (KPZ) universal scalings, in a controlled environment. The presented results are relevant to a wide range of photonic platforms sustaining Bose–Einstein-like transitions, such as vertically emitting laser diodes [44], photon condensates [45], and plasmonic structures embedded in cavities [46]. Moreover, an intense research effort is currently focused on polaritons in 2D electron gases [47,48] or transition metal dichalcogenides [49,50] embedded in cavities. Our proposal of using negative mass states to facilitate the establishment of long-range order could prove useful to achieve stable condensation in these novel platforms.

2. THEORETICAL FRAMEWORK

We start with a theoretical description of polariton condensation showing the physical origin of the reservoir-induced modulational instability. Ignoring the spin degree of freedom, the condensate wavefunction $\psi(\mathbf{r}, t)$ can be described by a generalized Gross–Pitaevskii equation coupled to a rate equation for the exciton reservoir density $n_R(\mathbf{r}, t)$ [31]:

$$i\hbar \frac{\partial \psi}{\partial t} = \left[-\frac{\hbar^2 \Delta}{2m} + g|\psi|^2 + 2g_R n_R + \frac{i\hbar}{2} (R n_R - \gamma) \right] \psi, \quad (1)$$

$$\frac{\partial n_R}{\partial t} = P(\mathbf{r}) - (\gamma_R + R|\psi|^2) n_R, \quad (2)$$

where $P(\mathbf{r})$ is the pumping rate, m is the effective polariton mass at the condensate energy, γ and γ_R are the polariton and exciton loss rates, and R is the relaxation rate of the reservoir into the condensate. g and g_R are positive and describe the repulsive polariton–polariton and polariton–reservoir interaction constants.

The widely used adiabatic approximation assumes that the reservoir follows instantaneously the condensate dynamics and is expected to be accurate if the reservoir decay time γ_R^{-1} is the fastest time scale [51]. Under this condition, Eq. (2) reduces to $n_R(\mathbf{r}) = P(\mathbf{r})/(\gamma_R + R|\psi|^2)$. Reinjecting into Eq. (1) yields a modified Ginzburg–Landau equation [27] in which g is replaced by an effective interaction constant [29,30]:

$$g_{\text{eff}} = g - 2g_R \frac{\gamma P_{\text{th}}}{\gamma_R P}. \quad (3)$$

This means that, as far as the condensate dynamics is concerned, the coupling to the reservoir reduces to an effective interaction between polaritons. The condensate is then dynamically stable for repulsive interactions ($g_{\text{eff}} > 0$, defocusing effective nonlinearity), and dynamically unstable for attractive interactions ($g_{\text{eff}} < 0$, self-focusing effective nonlinearity).

This polariton instability can be interpreted as a reservoir-induced modulational instability as follows. A local increase of polariton density (due to a quantum or thermal fluctuation of the condensate, or to pump noise) induces a local depletion of the reservoir density via a spatial hole burning [31,52]. Such a depletion creates a potential well that further attracts the condensate polaritons, making the initial fluctuation to exponentially grow in time. This positive feedback loop is eventually broken by gain saturation and by polariton propagation, so that the density fluctuation is ejected from its initial position and starts moving through the condensate. A turbulent behavior results from the chaotic evolution of several such density fluctuations [30,33,34].

In typical polariton experiments [53–58], $g \sim 0.05\text{--}0.5g_R$ and $\gamma \sim 10\text{--}100\gamma_R$, so that the stability condition $g_{\text{eff}} > 0$ requires high pump powers $P \sim 40\text{--}4000P_{\text{th}}$, difficult to achieve in practice, in particular for large pump spots in a CW regime. This stability condition can be relaxed by using a relatively small pumping spot ($\sim 2\text{--}10 \mu\text{m}$) [33,35,59], as was done in most previous experimental studies [53–58,60]. In that case, the confinement-induced kinetic energy and, possibly, the outwards flow due to the overall density profile compete with attractive interactions so that stable condensates can be achieved even for negative g_{eff} . But this method imposes small condensate sizes, which limits the capacity of polaritons to serve as a platform for simulating novel driven-dissipative phenomena [36–43]. A promising alternative are the large condensates recently demonstrated in cavities with long lifetimes and reduced wedge [61]. However, the fact that the condensate is fed by ballistically expanding fast polaritons instead of (almost) immobile excitons introduces a more complex spatial dynamics into the reservoir Eq. (2), which is likely to modify the universal properties of the transition.

In contrast to all these works, here we demonstrate how the dynamical instability of condensates under CW pumping with a large spot ($\approx 90 \mu\text{m}$) can be tamed by introducing a periodic potential. When condensation occurs in negative mass states, stable condensates of arbitrarily large size (limited only by the available total pump power) can be obtained while maintaining a coupling to an excitonic reservoir of the standard form in Eq. (2), for which rich KPZ driven-dissipative phase transitions are expected [38,39,41–43].

3. SAMPLES AND EXPERIMENTAL SETUP

Our microcavities, grown by molecular beam epitaxy, consist of a $\lambda/2$ Ga_{0.05}Al_{0.95}As layer surrounded by two

$\text{Ga}_{0.8}\text{Al}_{0.2}\text{As}/\text{Ga}_{0.05}\text{Al}_{0.95}\text{As}$ Bragg mirrors. To vary the quality factor, we fabricate two sets of cavities: (1) moderate Q factor with 26 and 30 pairs in the top/bottom mirrors, respectively, yielding a nominal quality factor $Q = 30000$; and (2) high Q factor with 28 and 40 pairs in the top/bottom mirrors, yielding nominally $Q = 70000$. For both types of cavities, 12 GaAs quantum wells of width 7 nm are inserted into the structure, resulting in a 15 meV Rabi splitting. The planar cavities are studied as such, or patterned into ridges or lattices of coupled micropillars, by e-beam lithography followed with dry etching (down to the GaAs substrate).

In the experiments described below, polaritons are excited non-resonantly with a CW monomode laser tuned to 740 nm. The sample temperature is 6 K and the cavity-exciton detuning is -10 meV (defined as the difference between the lowest-energy cavity mode and the exciton resonance). The polariton emission is collected with a 0.5 numerical aperture objective and focused on the entrance slit of a spectrometer coupled to a charge-coupled device camera. Imaging of the sample surface (resp. the Fourier plane) allows studying polariton properties in real (resp. reciprocal) space.

4. EXPERIMENTAL RESULTS IN 1D CAVITIES

We first consider 1D cavities, and we investigate polariton condensation in positive mass states. A wire cavity [width $3\ \mu\text{m}$ and length $200\ \mu\text{m}$, see Fig. 1(a)] of moderate Q factor is excited with an elliptical spot of length $90\ \mu\text{m}$ (intensity full width at half maximum). Figure 1(b) shows the far-field emission at very low pump power [for the transverse magnetic (TM) polarization, i.e., parallel to the wire axis], evidencing a parabolic-like dispersion (near $k = 0$) with an effective mass $m \simeq 5 \times 10^{-5} m_0$ (m_0 is the free electron mass). When increasing the pump power, stimulated scattering causes the emission to collapse into a narrow spectral line [53] centered at $k = 0$, as seen in the spectrum of Fig. 1(c) obtained at $P = 2P_{\text{th}}$. The real-space image of the resulting polariton condensate [Fig. 1(d)] and the corresponding spatial profile [Fig. 1(f), black line] reveal inhomogeneity in the condensate density, with a typical contrast (ratio between

maximum and minimum density) $\mathcal{C} \simeq 2$ at the center of the pump spot.

To investigate the coherence properties of the condensate, we employ Michelson interferometry [53]. We superpose the condensate image with its mirror symmetric, obtained by reflection on a retroreflector, so that each point x of the condensate interferes with the point located at $-x$. The corresponding interferogram is shown in Fig. 1(e), for zero temporal delay ($t = 0$) between the two arms of the interferometer. By extracting the fringe visibility through Fourier analysis, we obtain the first-order spatial coherence $g^{(1)}(x, -x, t = 0)$, which is plotted in Fig. 1(f) (red line). The measured coherence extends over a much shorter length scale than the condensate density, with a coherence length (at $1/e$) of $l_c = 6\ \mu\text{m}$. This short spatial coherence is a first hint of the presence of an instability and of the consequent turbulent behavior. To gain further insight into this phenomenon, we investigate the temporal coherence. Figure 1(l) (green line) shows the evolution of $g^{(1)}(x = 0)$ when scanning the temporal delay t of the interferometer. The decay is non-monotonic (a revival is seen near $t = 40$ ps, see Supplement 1) and the envelope decays within a coherence time $\tau_c \simeq 50$ ps.

The density inhomogeneity [Fig. 1(f)] suggests that disorder is playing an important role in the experiment, leading to a significant spatial modulation of the condensate. We expect this effect to be amplified if the ratio between the disorder amplitude and the polariton linewidth increases (see discussion at the end of Section 5). To test this dependence, we perform the same set of experiments in a wire of high Q factor but similar disorder strength. The real-space image [Fig. 1(h)] and spatial profile [Fig. 1(j), black] of a condensate at $P = 2P_{\text{th}}$ indeed reveal a much stronger density inhomogeneity, with a typical contrast $\mathcal{C} \sim 10$: the condensate fragments into distinct lobes. The interferogram [Fig. 2(i)] and extracted spatial $g^{(1)}$ [Fig. 2(j), red] demonstrate that there is no mutual coherence between the different lobes of the condensate. Hence, the coherence length is limited to the lobe size and is of the order of $l_c = 8\ \mu\text{m}$, comparable to the one of the moderate Q condensate of Fig. 1(f). The coherence time, on the other hand, is here twice longer with $\tau_c \simeq 120$ ps for each lobe [Fig. 1(l), blue line].

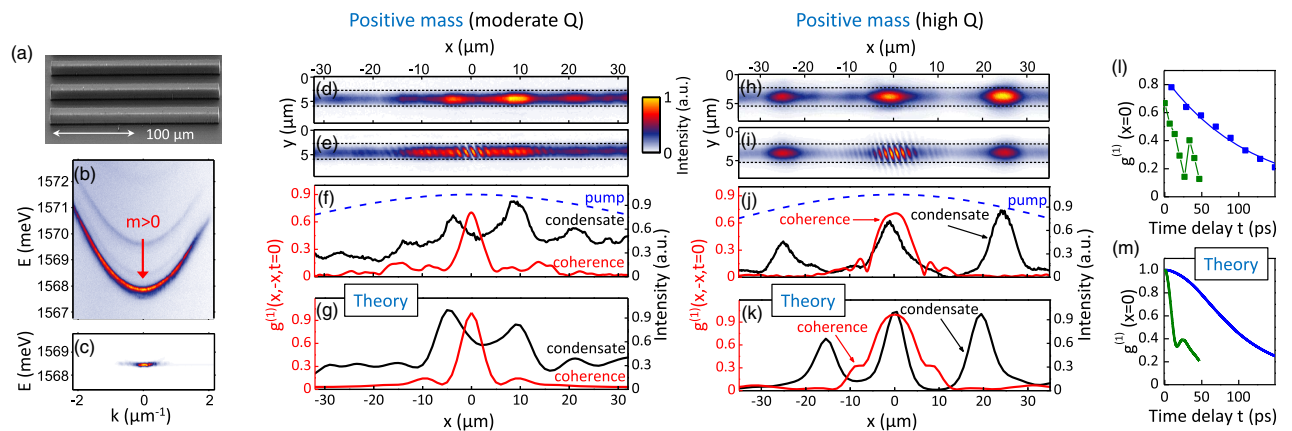


Fig. 1. (a) Scanning electron micrograph of 1D wire cavities. (b)–(c) Far-field emission (TM polarization) of a moderate Q wire cavity at pump power (b) below and (c) above the condensation threshold ($P = 2P_{\text{th}}$). (d) Real space image of the condensate. (e) Interferogram obtained by superposing two mirror-symmetric images of the condensate in a Michelson interferometer. (f) Measured and (g) calculated spatial coherence $g^{(1)}$ at $t = 0$ (red), compared to the spatial profile of the condensate (black) and of the pump spot (blue). (h)–(k) Same quantities as (d)–(g) obtained in a high Q wire cavity. (l) Measured and (m) calculated evolution of the $x = 0$ temporal coherence, for the moderate (green line) and high Q wire cavity (blue line).

Let us now investigate condensation in negative mass states, as it can be achieved by patterning the cavity into a lattice [62–64]. Our intuition is here guided by the adiabatic approximation, which led to the derivation of Eq. (3) for the effective interaction g_{eff} between polaritons. In this approximation, one can easily show that, all other parameters kept the same, inverting the sign of the mass reverses the effect of interactions [22–24], suppressing the feedback loop at the heart of the modulational instability.

To test this prediction, we fabricate a 1D Lieb lattice of coupled micropillars [65], as shown in Fig. 2(a). We here present data for a moderate Q cavity, but we obtained similar results at high Q . Each pillar has a diameter of $3\ \mu\text{m}$, and the lattice period is $a = 5.8\ \mu\text{m}$. The fundamental (s -symmetry) states of the pillars hybridize to form three bands. For our lattice parameters, the two lowest are superimposed within the linewidth, but the upper band is well separated, as seen in the far-field emission of Fig. 2(b) (TM polarization). This upper band shows a negative curvature at the center of the second Brillouin zones ($k = \pm 2\pi/a$, see vertical red arrows), yielding a negative effective mass $m \simeq -4 \times 10^{-5} m_0$ nearly equal to the opposite of the mass of the wire cavities studied above [66]. Figure 2(c) shows the condensate far-field emission at $P = 1.5P_{\text{th}}$, which is concentrated at the top of the upper band. The real-space image [Fig. 2(d)] and corresponding spatial profile [Fig. 2(f), black] show that the condensate possesses a regular Gaussian-like envelope, the disorder inducing only a minor modulation. The spatial coherence at $t = 0$, extracted from the interferogram of Fig. 2(e), is shown in Fig. 2(f) (red circles). As the antisymmetric character of the upper band makes the condensate density vanish in between neighboring pillars, we restricted our spatial sampling of the $g^{(1)}$ coherence function to the center of the pillars. We observe that the spatial coherence extends over the whole condensate, yielding a coherence length $l_c \simeq 35\ \mu\text{m}$, about five times higher than for positive mass condensates [Figs. 1(f) and 1(j)]. The temporal coherence $g^{(1)}(x = 0, t)$, shown in Fig. 2(h), reveals a slow and monotonic decay with a long coherence time $\tau_c \simeq 210\ \text{ps}$, four times higher than the one of the wire cavity of the same Q factor [Fig. 1(l), green]. This strongly suggests that the condensate is here dynamically stable.

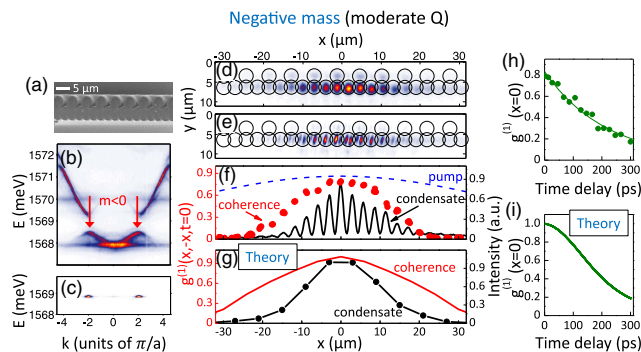


Fig. 2. (a) Scanning electron micrograph of a 1D Lieb lattice of micropillars. (b)–(c) Far-field emission (TM polarization) of a moderate Q Lieb lattice at pump power (b) below and (c) above the condensation threshold ($P = 1.5P_{\text{th}}$). (d) Real space image and (e) interferogram of the condensate. Positions of the micropillars are indicated by black circles. (f) Measured and (g) calculated spatial coherence $g^{(1)}$ at $t = 0$ (red), compared to the spatial profile of the condensate (black) and of the pump spot (blue). (h) Measured and (i) calculated evolution of the $x = 0$ temporal coherence.

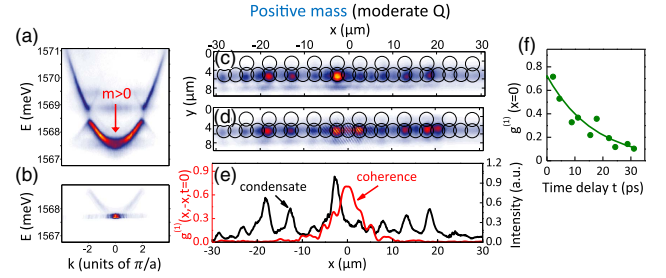


Fig. 3. (a)–(b) Far-field emission of a moderate Q Lieb lattice at pump power (a) below and (b) above the condensation threshold ($P = 1.5P_{\text{th}}$) when condensation is triggered into a positive mass state. (c) Real-space image and (d) interferogram of the condensate. (e) Measured spatial coherence $g^{(1)}$ at $t = 0$ (red), compared to the spatial profile of the condensate (black). (f) Measured evolution of the $x = 0$ temporal coherence.

To verify that the high coherence and homogeneity are due the negative mass, and not simply to the patterning of the cavity into micropillars, we also consider condensation in a positive mass state of the lattice. For this, we use a lattice with slightly reduced cavity-exciton detuning ($-8\ \text{meV}$ instead of $-10\ \text{meV}$) so as to enhance the relaxation of polaritons towards the fundamental state. In this condition, condensation is triggered at the bottom of the lower energy band, as shown in the far-field spectrum of Fig. 3(b) (power $P = 1.5P_{\text{th}}$, lattice period $a = 5.2\ \mu\text{m}$). This positive mass condensate is highly inhomogeneous [Figs. 3(c) and 3(e)] and has short spatial coherence [Figs. 3(d) and 3(e)] [67], similar to the positive mass condensates observed in 1D wires (Fig. 1). Furthermore, the coherence time $\tau_c \simeq 20\ \text{ps}$ [Fig. 3(f)] is one order of magnitude smaller than for the negative mass condensate [Fig. 2(h)]. Hence, the patterning of a cavity into a lattice of micropillars is not sufficient to obtain homogeneous and highly coherent condensates. These are obtained only when condensation occurs in negative mass states.

Finally, a further evidence in support of our interpretation is obtained by comparison to the case of condensation in a flat energy band, which we have reported previously [65]. Since the effective mass is infinite, kinetic energy is suppressed in this case: density fluctuations cannot propagate, and the instability mechanism described here is quenched. A condensate with homogeneous profile is thus obtained, but strongly reduced spatial coherence reveals the fragmentation of the condensate into elementary plaquettes.

5. NUMERICAL SIMULATIONS

To get further physical insight into these condensation behaviors, let us now compare these experimental results to theoretical predictions. We start from a linear stability analysis of the time-independent steady state, assuming a spatially homogeneous system. Using parameters taken from the experiment, we calculate the spectrum $\omega(k)$ of the elementary (Bogoliubov) excitations (see Supplement 1). We first consider the adiabatic approximation, which has been widely used in the literature to describe various polaritonic experiments employing small excitation spots. Figure 4(a) shows the imaginary part of the spectrum for the positive mass condensate in the moderate Q wire cavity. In the low wavevector region, the upper Goldstone branch takes positive

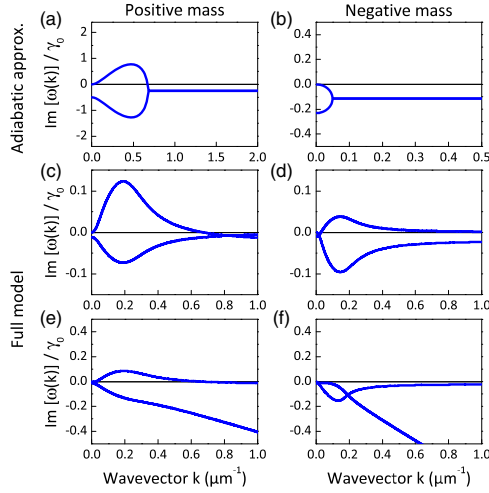


Fig. 4. (a)–(b) Imaginary part of the Bogoliubov excitation spectrum calculated under the adiabatic approximation, for a positive (a) and negative (b) mass condensate of moderate Q factor, assuming a constant polariton linewidth γ_0 . (c)–(f) Same quantities calculated with the full model of coupled Eqs. (1),(2), with a constant linewidth (c, d) and with a momentum-dependent linewidth (e, f). Formulas and parameters are given in the Supplement 1.

imaginary values: perturbations at these wavevectors are exponentially amplified by the system, corresponding to a modulationally unstable regime of condensation. Figure 4(b) shows the spectrum calculated for the negative mass condensate in the moderate Q lattice: here, all excitation modes have a negative imaginary part and are thus exponentially damped, corresponding to a stable regime of condensation.

We now go beyond the adiabatic approximation by considering the full model formed by the coupled Eqs. (1),(2). As seen in Fig. 4(c), the qualitative shape of the spectrum for the positive mass condensate remains essentially unchanged, although quantitative values of the strength and wavevector for the onset of instability are modified. For the negative mass condensate, however [see Fig. 4(d)], the spectrum is qualitatively altered compared to the adiabatic approximation, and a novel instability appears. Such specifically non-adiabatic instability, not discussed previously in the literature, is *a priori* relevant given our experimental parameters, but is not observed in our measurements.

Several mechanisms can be invoked to explain the suppression of this new instability. In particular, in a lattice, the polariton linewidth is expected to be minimum in antisymmetric states [68,69]. In these states, the π phase difference of the wavefunction between neighboring sites leads to maximum polariton density in the center of the pillars and zero density in the region in between micropillars. It is in this region that non-radiative losses arising from surface defects generated during the etching process present a higher density. Therefore, antisymmetric states are expected to have the longest lifetime. In our case [see Fig. 2(b)] condensation occurs in such antisymmetric states located in the upper band at the center of the Brillouin zones. The linewidth is then expected to increase monotonically away from the zone centers as the phase difference between neighboring sites progressively departs from π , leading to higher probability density in between micropillars and thus broader polariton linewidth. In our experiments we can quantify this phenomenon by extracting the linewidth of

the low-power photoluminescence as a function of the wavevector k (see Supplement 1, Fig. S5). In the upper band we find an approximate linear increase of the linewidth, $\gamma(k) = \gamma_0 + \gamma'|k|$, with $\hbar\gamma_0 = 75(130) \mu\text{eV}$ for high (moderate) Q lattices, and $\gamma'/\gamma_0 \simeq 1.6 \mu\text{m}$. When introducing such momentum-dependent linewidth in the simulations, the instability is indeed suppressed, as shown in the spectrum of Fig. 4(f). For the 1D wire cavities, photoluminescence measurements also reveal a slight k -dependency of the linewidth, $\gamma'/\gamma_0 \simeq 0.7 \mu\text{m}$, which could be linked to energy relaxation effects [70]. For completeness, we include this effect in the simulations of the positive mass condensate as well: as shown in Fig. 4(e), the condensate remains in the unstable regime.

To go beyond the stability analysis and simulate the spatial and temporal coherence of the condensate, we now consider the full nonlinear model of Eqs. (1),(2), including the k -dependent linewidth and the pump profile. We add a Gaussian noise term to Eq. (1) so as to effectively account for all quantum, thermal, or pump laser fluctuations, as well as a disorder potential with a standard deviation of $30 \mu\text{eV}$ corresponding to the typical disorder strength of our cavities [65]. The shape of the disorder is adjusted to fit the experimentally observed condensate density profiles [e.g., Figs. 1(f) and 1(j)]. Figures 1(g) and 1(k) show the simulated time-averaged condensate density (black) and spatial coherence at $t = 0$ (red) for the positive mass condensate, for moderate and high Q wire cavities. Figure 1(m) shows the corresponding temporal coherence, all in good agreement with the experiment.

The observed difference between moderate and high Q cavities can be intuitively understood from the interplay between instability and disorder. At moderate Q , density fluctuations chaotically propagate along the condensate, resulting in a strongly reduced spatial and temporal coherence: the non-monotonicity in the temporal coherence [Fig. 1(l) and 1(m), green line] arises from the scattering of density fluctuations on the disorder. At high Q , on the contrary, due to the higher disorder/linewidth ratio, density fluctuations are pinned into localized high-density areas, which strongly constrains their dynamics and thus their ability to spoil the temporal coherence [Figs. 1(l) and 1(m), blue line]. Note that a similar interplay between nonlinearity, dissipation, and disorder is encountered in the instability of multimode fibers [5] and random lasers [71].

Now turning to negative mass condensates, we calculate their spatio-temporal coherence by considering the highest energy band of the Lieb lattice in the tight-binding limit [69], and we introduce disorder with the same amplitude as for positive mass. Figures 2(g) and 2(i) show the spatial coherence at zero delay ($g^{(1)}(x, 0)$) and the time decay of the coherence ($g^{(1)}(0, t)$). The simulations show a smooth density profile and a high spatial and temporal coherence, in good agreement with the experimental results [Figs. 2(f) and 2(h)].

6. EXPERIMENTAL RESULTS IN 2D CAVITIES

The physical mechanism of the polariton instability is expected to be independent of the dimensionality of the system (except at 0D, where any dynamics is quenched) [31]. We have reported above a complete set of data obtained in 1D systems, motivated by the convenience in measuring and calculating coherence properties in these systems, but similar results are expected in 2D cavities. To test this prediction we have performed spatial coherence measurements in 2D cavities, as reported in Fig. 5. The exciton

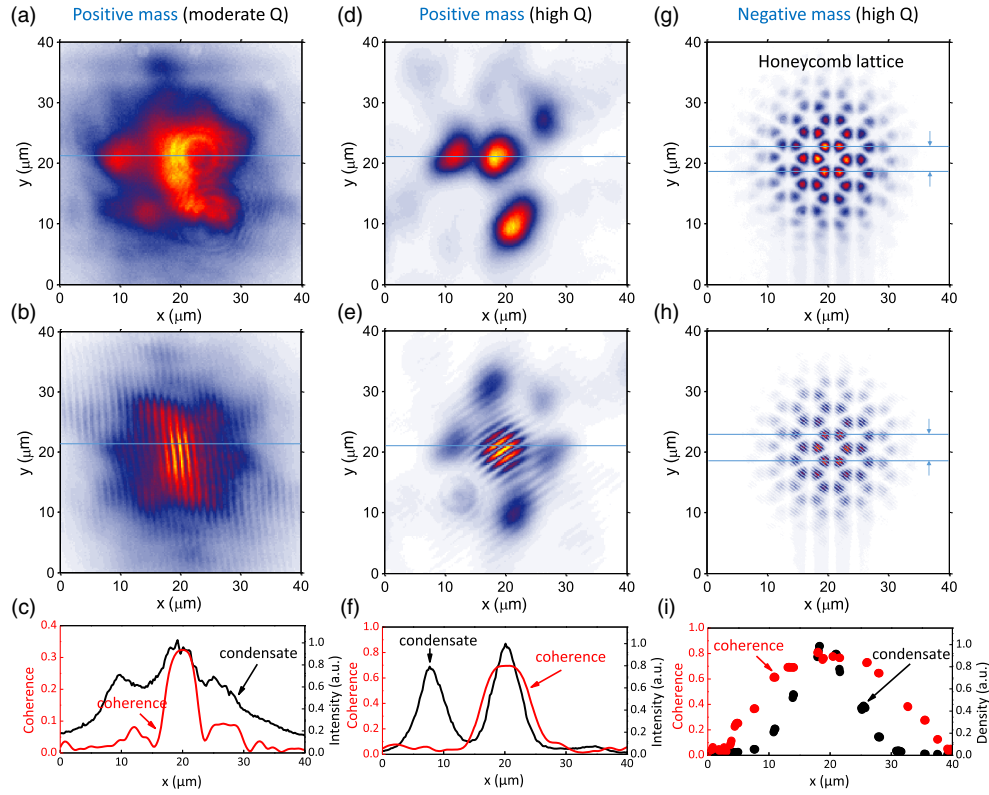


Fig. 5. Condensation in 2D cavities. (a) Real-space image and (b) interferogram of the condensate in a planar cavity with moderate Q factor. (c) Cuts of the condensate density and of the spatial coherence profiles along the horizontal axis indicated in (a)–(b). (d)–(f) Similar measurements performed on a high Q planar cavity. (g)–(i) Similar measurements performed on a high Q honeycomb lattice of coupled micropillars.

detuning, polariton mass, and normalized pump power $P/P_{\text{th}} \approx 2$ are similar to those used for 1D cavities.

The first two columns of Fig. 5 compare results obtained, respectively, in planar cavities of moderate and high Q factors, excited by a circular Gaussian pump spot with $60 \mu\text{m}$ radius (we used a smaller size spot than for 1D experiments because of power density limitation). From top to bottom are shown: the real-space image of the condensate, the interferogram obtained by superimposing two mirror-symmetric images, and spatial profiles of the condensate density and coherence along the axes indicated by blue horizontal lines.

For the moderate Q planar cavity (first column), the condensate extends on about $25 \times 25 \mu\text{m}^2$ and shows slight density inhomogeneity [black line in Fig. 5(c)], with a contrast $\mathcal{C} \approx 2$. The spatial coherence [red line in Fig. 5(c)] extends on a much shorter scale ($l_c \sim 6 \mu\text{m}$) than the condensate density, which indicates the presence of an instability with signatures comparable to the 1D moderate Q wire cavity studied in Fig. 1(f).

Now turning to measurements performed in a high Q planar cavity (second column of Fig. 5), we observe a strong increase of the density inhomogeneity of the condensate, with a typical contrast $\mathcal{C} \approx 10$. The condensate fragments into distinct lobes, with no mutual coherence between them [Fig. 5(f), red]: the coherence length is on the order of the lobe size, $l_c \approx 10 \mu\text{m}$. These data corroborate the evidence for a fragmentation regime of the polariton instability at high Q factors, similar to the 1D case [Fig. 1(j)].

Finally, in the last column of Fig. 5 we investigate condensation in a negative mass state, by using a 2D honeycomb lattice of

micropillars (high Q factor and interpillar spacing $2.4 \mu\text{m}$) [62]. Condensation here occurs at the top edge of the π^* band, thus in a negative mass quantum state. The honeycomb-shaped spatial distribution of the condensate reflects the lattice geometry. Here, we integrate the density and coherence over the three central pillar rows (see horizontal lines). The envelope slowly decays following a smooth Gaussian-like profile [black points in Fig. 5(i)], despite the presence of disorder with a similar amplitude as in the planar cavities. The spatial coherence [red points in Fig. 5(f)] extends over the whole condensate, with a coherence length $l_c \approx 35 \mu\text{m}$ about four times higher than for positive mass condensates [Figs. 5(c) and 5(f)], pointing out a stable regime of condensation. Note that the size of the condensates cannot be made larger in these experiments because of limited available excitation density.

7. CONCLUSION

In summary, we have reported a comprehensive study of polariton condensation in III-V cavities, by varying the sign of the effective mass, the dimensionality, and the cavity Q factor. Due to effective attractive interactions mediated by the exciton reservoir, positive mass condensates are dynamically unstable as evidenced by a strongly reduced spatial and temporal coherence and a spatially inhomogeneous density. Using a lattice to invert the sign of the polariton mass allows to suppress this instability and prepare extended condensates with high spatial and temporal coherence. This method opens exciting possibilities in view of investigating novel driven-dissipative phenomena [36–43] with bosonic condensates in a controlled platform.

Funding. Agence Nationale de la Recherche (ANR) (ANR-16-CE30-0021); Labex NanoSaclay (ANR-10-LABX-0035); French RENATECH network; H2020 European Research Council (ERC) (Honeypol); H2020 Future and Emerging Technologies (FET) (640800); Austrian Science Fund (FWF) (DK CoQuS W 1210, SFB FOQUS F40, Y 591-N16).

See Supplement 1 for supporting content.

REFERENCES AND NOTES

1. T. B. Benjamin and J. Feir, "The disintegration of wave trains on deep water," *J. Fluid Mech.* **27**, 417–430 (1967).
2. K. Tai, A. Hasegawa, and A. Tomita, "Observation of modulational instability in optical fibers," *Phys. Rev. Lett.* **56**, 135–138 (1986).
3. F. Amiranoff, M. Laberge, J. Marques, F. Moulin, E. Fabre, B. Cros, G. Matthieussent, P. Benkheiri, F. Jacquet, J. Meyer, P. Miné, C. Stenz, and P. Mora, "Observation of modulational instability in Nd-laser beat-wave experiments," *Phys. Rev. Lett.* **68**, 3710–3713 (1992).
4. K. E. Strecker, G. B. Partridge, A. G. Truscott, and R. G. Hulet, "Formation and propagation of matter-wave soliton trains," *Nature* **417**, 150–153 (2002).
5. L. G. Wright, Z. Liu, D. A. Nolan, M.-J. Li, D. N. Christodoulides, and F. W. Wise, "Self-organized instability in graded-index multimode fibres," *Nat. Photonics* **10**, 771–776 (2016).
6. G. I. Stegeman and M. Segev, "Optical spatial solitons and their interactions: universality and diversity," *Science* **286**, 1518–1523 (1999).
7. S. Hegarty, G. Huyet, J. McInerney, and K. Choquette, "Pattern formation in the transverse section of a laser with a large Fresnel number," *Phys. Rev. Lett.* **82**, 1434–1437 (1999).
8. M. Sciamanna and K. A. Shore, "Physics and applications of laser diode chaos," *Nat. Photonics* **9**, 151–162 (2015).
9. F. Selmi, S. Coulibaly, Z. Loghmari, I. Sagnes, G. Beaudoin, M. G. Clerc, and S. Barbay, "Spatiotemporal chaos induces extreme events in an extended microcavity laser," *Phys. Rev. Lett.* **116**, 013901 (2016).
10. K. Hammani, C. Finot, J. M. Dudley, and G. Millot, "Optical rogue-wave-like extreme value fluctuations in fiber Raman amplifiers," *Opt. Express* **16**, 16467–16474 (2008).
11. L. F. Mollenauer, R. H. Stolen, and J. P. Gordon, "Experimental observation of picosecond pulse narrowing and solitons in optical fibers," *Phys. Rev. Lett.* **45**, 1095–1098 (1980).
12. M. Carvalho, S. Singh, and D. Christodoulides, "Modulational instability of quasi-plane-wave optical beams biased in photorefractive crystals," *Opt. Commun.* **126**, 167–174 (1996).
13. D. Solli, C. Ropers, P. Koonath, and B. Jalali, "Optical rogue waves," *Nature* **450**, 1054–1057 (2007).
14. F. Arecchi, R. Meucci, G. Puccioni, and J. Tredicce, "Experimental evidence of subharmonic bifurcations, multistability, and turbulence in a Q-switched gas laser," *Phys. Rev. Lett.* **49**, 1217–1220 (1982).
15. J. L. Roberts, N. R. Claussen, S. L. Cornish, E. A. Donley, E. A. Cornell, and C. E. Wieman, "Controlled collapse of a Bose-Einstein condensate," *Phys. Rev. Lett.* **86**, 4211–4214 (2001).
16. E. A. Donley, N. R. Claussen, S. L. Cornish, J. L. Roberts, E. A. Cornell, and C. E. Wieman, "Dynamics of collapsing and exploding Bose-Einstein condensates," *Nature* **412**, 295–299 (2001).
17. L. P. Pitaevskii and S. Stringari, *Bose-Einstein Condensation and Superfluidity* (Oxford University, 2016).
18. H. T. C. Stoof, "Atomic Bose gas with a negative scattering length," *Phys. Rev. A* **49**, 3824–3830 (1994).
19. J. M. Gerton, D. Strekalov, I. Prodan, and R. G. Hulet, "Direct observation of growth and collapse of a Bose-Einstein condensate with attractive interactions," *Nature* **408**, 692–695 (2000).
20. T. Lahaye, J. Metz, B. Fröhlich, T. Koch, M. Meister, A. Griesmaier, T. Pfau, H. Saito, Y. Kawaguchi, and M. Ueda, "d-wave collapse and explosion of a dipolar Bose-Einstein condensate," *Phys. Rev. Lett.* **101**, 080401 (2008).
21. J. H. Nguyen, D. Luo, and R. G. Hulet, "Formation of matter-wave soliton trains by modulational instability," *Science* **356**, 422–426 (2017).
22. R. Boyd, *Nonlinear Optics* (Academic, 1992).
23. P. Butcher and D. Cotter, *The Elements of Nonlinear Optics* (Cambridge University, 1993).
24. C. M. de Sterke and J. Sipe, *Progress in Optics XXXIII* (Elsevier, 1994), pp. 203–260.
25. T. Anker, M. Albiez, R. Gati, S. Hunsmann, B. Eiermann, A. Trombettoni, and M. Oberthaler, "Nonlinear self-trapping of matter waves in periodic potentials," *Phys. Rev. Lett.* **94**, 020403 (2005).
26. M. Khomechi, K. Hossain, M. Mossman, Y. Zhang, T. Busch, M. M. Forbes, and P. Engels, "Negative-mass hydrodynamics in a spin-orbit-coupled Bose-Einstein condensate," *Phys. Rev. Lett.* **118**, 155301 (2017).
27. I. Carusotto and C. Ciuti, "Quantum fluids of light," *Rev. Mod. Phys.* **85**, 299–366 (2013).
28. C. Ciuti, V. Savona, C. Piermarocchi, A. Quattropani, and P. Schwendimann, "Role of the exchange of carriers in elastic exciton-exciton scattering in quantum wells," *Phys. Rev. B* **58**, 7926–7933 (1998).
29. L. A. Smirnov, D. A. Smirnova, E. A. Ostrovskaya, and Y. S. Kivshar, "Dynamics and stability of dark solitons in exciton-polariton condensates," *Phys. Rev. B* **89**, 235310 (2014).
30. T. C. H. Liew, O. A. Egorov, M. Matuszewski, O. Kyriienko, X. Ma, and E. A. Ostrovskaya, "Instability-induced formation and nonequilibrium dynamics of phase defects in polariton condensates," *Phys. Rev. B* **91**, 085413 (2015).
31. M. Wouters and I. Carusotto, "Excitations in a nonequilibrium Bose-Einstein condensate of exciton polaritons," *Phys. Rev. Lett.* **99**, 140402 (2007).
32. J. Cuevas, A. S. Rodrigues, R. Carretero-González, P. G. Kevrekidis, and D. J. Frantzeskakis, "Nonlinear excitations, stability inversions, and dissipative dynamics in quasi-one-dimensional polariton condensates," *Phys. Rev. B* **83**, 245140 (2011).
33. N. Bobrovskaya, E. A. Ostrovskaya, and M. Matuszewski, "Stability and spatial coherence of nonresonantly pumped exciton-polariton condensates," *Phys. Rev. B* **90**, 205304 (2014).
34. N. Bobrovskaya and M. Matuszewski, "Adiabatic approximation and fluctuations in exciton-polariton condensates," *Phys. Rev. B* **92**, 035311 (2015).
35. N. Bobrovskaya, M. Matuszewski, K. S. Daskalakis, S. A. Maier, and S. Kéna-Cohen, "Dynamical instability of a nonequilibrium exciton-polariton condensate," *ACS Photon.* **5**, 111–118 (2018).
36. L. M. Sieberer, S. D. Huber, E. Altman, and S. Diehl, "Dynamical critical phenomena in driven-dissipative systems," *Phys. Rev. Lett.* **110**, 195301 (2013).
37. A. Chiocchetta and I. Carusotto, "Non-equilibrium quasi-condensates in reduced dimensions," *Europhys. Lett.* **102**, 67007 (2013).
38. L. He, L. M. Sieberer, E. Altman, and S. Diehl, "Scaling properties of one-dimensional driven-dissipative condensates," *Phys. Rev. B* **92**, 155307 (2015).
39. E. Altman, L. M. Sieberer, L. Chen, S. Diehl, and J. Toner, "Two-dimensional superfluidity of exciton polaritons requires strong anisotropy," *Phys. Rev. X* **5**, 011017 (2015).
40. G. Dagvadorj, J. M. Fellows, S. Matyjaśkiewicz, F. M. Marchetti, I. Carusotto, and M. H. Szymańska, "Nonequilibrium phase transition in a two-dimensional driven open quantum system," *Phys. Rev. X* **5**, 041028 (2015).
41. V. N. Gladilin, K. Ji, and M. Wouters, "Spatial coherence of weakly interacting one-dimensional nonequilibrium bosonic quantum fluids," *Phys. Rev. A* **90**, 023615 (2014).
42. K. Ji, V. N. Gladilin, and M. Wouters, "Temporal coherence of one-dimensional nonequilibrium quantum fluids," *Phys. Rev. B* **91**, 045301 (2015).
43. D. Squizzato, L. Canet, and A. Minguzzi, "Kardar-Parisi-Zhang universality in the phase distributions of one-dimensional exciton-polaritons," arXiv:1712.03709 (2017).
44. L. Lundeberg, G. Lousberg, D. Boiko, and E. Kapon, "Spatial coherence measurements in arrays of coupled vertical cavity surface emitting lasers," *Appl. Phys. Lett.* **90**, 021103 (2007).
45. J. Klaers, J. Schmitt, F. Vewinger, and M. Weitz, "Bose-Einstein condensation of photons in an optical microcavity," *Nature* **468**, 545–548 (2010).
46. M. Ramezani, A. Halpin, A. I. Fernández-Domínguez, J. Feist, S. R.-K. Rodríguez, F. J. García-Vidal, and J. G. Rivas, "Plasmon-exciton-polariton lasing," *Optica* **4**, 31–37 (2017).
47. M. Sidler, P. Back, O. Cotlet, A. Srivastava, T. Fink, M. Kroner, E. Demler, and A. Imamoglu, "Fermi polaron-polaritons in charge-tunable atomically thin semiconductors," *Nat. Phys.* **13**, 255–261 (2017).

48. S. Ravets, P. Knüppel, S. Faelt, O. Cotlet, M. Kroner, W. Wegscheider, and A. Imamoglu, "Polaron polaritons in the integer and fractional quantum Hall regimes," *Phys. Rev. Lett.* **120**, 057401 (2018).
49. X. Liu, T. Galfsky, Z. Sun, F. Xia, E.-C. Lin, Y.-H. Lee, S. Kéna-Cohen, and V. M. Menon, "Strong light-matter coupling in two-dimensional atomic crystals," *Nat. Photonics* **9**, 30–34 (2015).
50. S. Dufferwiel, S. Schwarz, F. Withers, A. Trichet, F. Li, M. Sich, O. Del Pozo-Zamudio, C. Clark, A. Nalitov, D. Solnyshkov, G. Malpuech, K. S. Novoselov, J. M. Smith, M. S. Skolnick, D. N. Krizhanovskii, and A. I. Tartakovskii, "Exciton-polaritons in van der Waals heterostructures embedded in tunable microcavities," *Nat. Commun.* **6**, 8579 (2015).
51. More formally, three independent analytical conditions need to be fulfilled so as to apply the adiabatic approximation, as shown in Ref. [34].
52. E. Estrecho, T. Gao, N. Bobrovska, M. Fraser, M. Steger, L. Pfeiffer, K. West, T. Liew, M. Matuszewski, D. Snoke, A. G. Truscott, and E. A. Ostrovskaya, "Spontaneous condensation of exciton polaritons in the single-shot regime," arXiv:1705.00469 (2017).
53. J. Kasprzak, M. Richard, S. Kundermann, A. Baas, P. Jeambrun, J. Keeling, F. Marchetti, M. Szymańska, R. Andre, J. Staehli, V. Savona, P. B. Littlewood, B. Deveaud, and L. S. Dang, "Bose-Einstein condensation of exciton polaritons," *Nature* **443**, 409–414 (2006).
54. H. Deng, G. S. Solomon, R. Hey, K. H. Ploog, and Y. Yamamoto, "Spatial coherence of a polariton condensate," *Phys. Rev. Lett.* **99**, 126403 (2007).
55. F. Manni, K. G. Lagoudakis, R. André, M. Wouters, and B. Deveaud, "Penrose-Onsager criterion validation in a one-dimensional polariton condensate," *Phys. Rev. Lett.* **109**, 150409 (2012).
56. G. Roumpos, M. Lohse, W. H. Nitsche, J. Keeling, M. H. Szymańska, P. B. Littlewood, A. Löffler, S. Höfling, L. Worschech, A. Forchel, and Y. Yamamoto, "Power-law decay of the spatial correlation function in exciton-polariton condensates," *Proc. Natl. Acad. Sci. USA* **109**, 6467–6472 (2012).
57. W. H. Nitsche, N. Y. Kim, G. Roumpos, C. Schneider, M. Kamp, S. Höfling, A. Forchel, and Y. Yamamoto, "Algebraic order and the Berezinskii-Kosterlitz-Thouless transition in an exciton-polariton gas," *Phys. Rev. B* **90**, 205430 (2014).
58. J. Fischer, I. G. Savenko, M. D. Fraser, S. Holzinger, S. Brodbeck, M. Kamp, I. A. Shelykh, C. Schneider, and S. Höfling, "Spatial coherence properties of one dimensional exciton-polariton condensates," *Phys. Rev. Lett.* **113**, 203902 (2014).
59. K. S. Daskalakis, S. A. Maier, and S. Kéna-Cohen, "Spatial coherence and stability in a disordered organic polariton condensate," *Phys. Rev. Lett.* **115**, 035301 (2015).
60. H. Ohadi, E. Kammann, T. C. H. Liew, K. G. Lagoudakis, A. V. Kavokin, and P. G. Lagoudakis, "Spontaneous symmetry breaking in a polariton and photon laser," *Phys. Rev. Lett.* **109**, 016404 (2012).
61. D. Ballarini, D. Caputo, C. S. Muñoz, M. De Giorgi, L. Dominici, M. H. Szymańska, K. West, L. N. Pfeiffer, G. Gigli, F. P. Laussy, and D. Sanvitto, "Macroscopic two-dimensional polariton condensates," *Phys. Rev. Lett.* **118**, 215301 (2017).
62. T. Jacqmin, I. Carusotto, I. Sagnes, M. Abbarchi, D. D. Solnyshkov, G. Malpuech, E. Galopin, A. Lemaître, J. Bloch, and A. Amo, "Direct observation of Dirac cones and a flatband in a honeycomb lattice for polaritons," *Phys. Rev. Lett.* **112**, 116402 (2014).
63. S. Klembt, T. H. Harder, O. A. Egorov, K. Winkler, H. Suchomel, J. Beierlein, M. Emmerling, C. Schneider, and S. Höfling, "Polariton condensation in s- and p-flatbands in a two-dimensional Lieb lattice," *Appl. Phys. Lett.* **111**, 231102 (2017).
64. C. Whittaker, E. Cancellieri, P. Walker, D. Gulevich, H. Schomerus, D. Vaitiekus, B. Royall, D. Whittaker, E. Clarke, I. Iorsh, I. A. Shelykh, M. S. Skolnick, and D. N. Krizhanovskii, "Exciton polaritons in a two-dimensional Lieb lattice with spin-orbit coupling," *Phys. Rev. Lett.* **120**, 097401 (2018).
65. F. Baboux, L. Ge, T. Jacqmin, M. Biondi, E. Galopin, A. Lemaître, L. Le Gratiet, I. Sagnes, S. Schmidt, H. E. Türeci, A. Amo, and J. Bloch, "Bosonic condensation and disorder-induced localization in a flat band," *Phys. Rev. Lett.* **116**, 066402 (2016).
66. In our lattice, we note that due to the large interpillar spacing (required to obtain a band with large negative mass) the optical overlap between pillars is small. In this limit, the additional Lieb sites are only weakly coupled and play a minor role, so that the band structure resembles that of a simple linear chain of pillars of period $a' = a/2$. In the case of such a simple linear chain, there is a single band that takes a negative curvature at the edges of the Brillouin zone, located at $k = \pm\pi/a' = \pm 2\pi/a$, i.e., at the same absolute wavevector position than for the Lieb lattice we consider here.
67. The density of the interference fringes is fixed by the relative angle between both arms of the interferometer. In Figs. 3(d) and 5(h), we used for convenience a higher fringe density to be able to measure a sufficient number of fringes within the small spatial areas occupied by the condensate. This does not affect the fringe contrast, which is the only relevant quantity to extract the coherence.
68. I. L. Aleiner, B. L. Altshuler, and Y. G. Rubo, "Radiative coupling and weak lasing of exciton-polariton condensates," *Phys. Rev. B* **85**, 121301 (2012).
69. P. Stepnicki and M. Matuszewski, "Tight-binding model for exciton-polariton condensates in external potentials," *Phys. Rev. A* **88**, 033626 (2013).
70. C. Antón, T. C. H. Liew, G. Tosi, M. D. Martn, T. Gao, Z. Hatzopoulos, P. S. Eldridge, P. G. Savvidis, and L. Viña, "Energy relaxation of exciton-polariton condensates in quasi-one-dimensional microcavities," *Phys. Rev. B* **88**, 035313 (2013).
71. S. Mujumdar, V. Türck, R. Torre, and D. S. Wiersma, "Chaotic behavior of a random laser with static disorder," *Phys. Rev. A* **76**, 033807 (2007).